Laser Anemometer Measurements in a Compressor Rotor Flowfield at Off-Design Conditions

P. Popovski* and B. Lakshminarayana†
The Pennsylvania State University, University Park, Pennsylvania

The measurement of the flowfield at the peak pressure rise condition in an axial flow compressor rotor is reported in this paper. The inviscid flow measurement was carried out using a laser Doppler velocimeter and the blade boundary layers were measured using a two-sensor hot-wire pobe. The blade-to-blade distribution of velocities at several axial and radial locations are plotted, interpreted, and compared with the conditions existing at a lower (design) flow coefficient. The leading-edge effects on inviscid flow are found to be appreciable. The flowfield is dominated by inviscid flow at most radial locations and the blade boundary-layer thickness is found to be appreciable in the tip region. The flow near the tip is dominated by leakage and its influence is more severe at the peak pressure rise condition.

Nomenclature

C_L = local lift coefficient based on local inlet dynamic head of the relative flow
p, P_0 = static and stagnation pressure of absolute flow
PS, SS = pressure and suction surfaces, respectively
R = radius ratio, r/r_t
S = blade spacing
s,n,r = streamwise, normal, and radial coordinate directions
U_t = blade tip speed
V, W = absolute and relative flow velocity normalized by the blade tip speed
W_s = resultant velocity on the cylindrical surface, $\sqrt{(W_\theta^2 + W_z^2)}$
Y = tangential distance normalized by the local distance from blade to blade ($Y=0$ on suction side, $Y=1$ on pressure side)
Z = chordwise distance from the leading edge, normalized by local blade chord
z,θ,r = axial, tangential, and radial coordinate directions
α, β = absolute and relative flow angle measured from the axial direction
$\bar{\eta}$ = efficiency based on mass-averaged values
$\bar{\phi}$ = flow coefficient, $\bar{V}_z/U_t$
$\bar{\psi}$ = mass-averaged pressure rise coefficient (normalized by $2/\rho U_t^2$)
ψ_0 = $2(P_0 - p_a)/\rho U_t^2$
ψ_s = static pressure coefficient, $2(p - p_a)/\rho U_t^2$
ρ = air density

Subscripts

a = ambient conditions
s,n,r = values in streamwise, normal, and radial directions
z,θ,r = values in axial, tangential, and radial directions

Superscript

$\bar{(\ )}$ = blade-to-blade mass-averaged values

Introduction

In present-day turbomachinery, the three-dimensional inviscid and viscid effects play a very significant role in the accurate prediction of the performance or in the improvement of design techniques. A knowledge of the accurate flowfield is essential for the determination of the optimum performance and in the prediction of the off-design performance and onset of stall or surge. Several groups are actively working toward the computation of the entire flowfield in a rotor passage. These predictions can be used effectively and confidently only when the computational techniques are validated against the experimental data to determine their accuracy, range, and limitations. Some of the analyses[1-3] show good agreement with simple test cases or overall properties,[4,5] but the lack of adequate flowfield data has prevented verification of these theories for use in the design of turbomachines and in the predition of optimum and off-design performance. A comprehensive set of data inside a rotor, including the inviscid core flow and the blade boundary layer, is urgently needed. A set of data on the inviscid flowfield in a compressor rotor at the design point of operation measured from a five-hole probe has been reported in Ref. 5. The data on the blade boundary layer at the design point of operation, measured from a miniature two-sensor hot-wire probe, are reported in Ref. 6. The inviscid data inside a transonic rotor are reported in Ref. 4. None of these investigations provided a complete set of data for the entire rotor passage. The present work is the first set of data on the entire flowfield inside a compressor rotor, including the blade boundary layer at the off-design point of operation.

One of the major objectives of this investigation is to study the nature of the rotor flowfield from hub to tip and from leading to trailing edge, including the blade boundary layers on both surfaces of the blade. This should lead to a better understanding of the effects of off-design conditions of operation on the rotor flowfield. An additional objective is to obtain a comprehensive set of data necessary for the validation of the computer codes under development at Pennsylvania State University and elsewhere for the prediction of the entire inviscid and viscous flow in a turbomachinery rotor passage.

The present study includes measurements at six axial and five radial locations inside the rotor passage, a total of 30 blade-to-blade velocity profiles in the rotor passage at the

Received May 13, 1985; revision submitted Nov. 14, 1985.

*Fulbright Scholar, University of Skopje, Yugoslavia; presently Visiting Assistant Professor of Aerospace Engineering, Department of Aerospace Engineering.

†Distinguished Alumni Professor of Aerospace Engineering and Director of Computational Fluid Dynamics Studies, Department of Aerospace Engineering. Fellow AIAA.

off-design point of operation. Some of the data are presented and interpreted in this paper. The inviscid flow measurements are performed with a laser Doppler velocimeter (LDV) and the blade boundary-layer measurements are performed with a miniature two-sensor "V" hot-wire probe. The two sets of data are combined and the velocity profiles from blade to blade are obtained. The data at off-design condition are compared with the data at the design conditions.

Experimental Facility and Program

The measurements are carried out in a single-stage axial flow compressor facility described in Ref. 7. Design details of the blading and the rotor can be found in Ref. 8. Relevant blading parameters are listed in Table 1. The hub/outer annulus wall diameter ratio of the facility is 0.5, with the diameter of the outer annulus wall equal to 0.936 m. The inlet guide vane (IGV) row consists of 43 blades and the rotor of 21 blades. The rotor is driven by a 37 kW variable-speed motor. The rotor is followed by a stator row of 25 blades. Downstream of the stator there is an axial flow fan with a variable blade setting to control the pressure rise and the mass flow through the facility. Operating conditions and rotor specifications are as follows: flow coefficient based on the tip speed $\bar{\phi}=0.50$ (off-design), stage loading coefficient based on tip speed $\bar{\psi}=0.55$ (peak value), rotor speed of 1080 rpm, and tip clearance 2-2.5 mm. The overall performance of the rotor, efficiency, and $\bar{\psi}$ is shown in Fig. 1.

The rotating-probe traverse mechanism and the instrumentation system used for blade boundary-layer measurements are described in detail in Ref. 7. The circumferential traverse can be accomplished when the rotor is rotating. The step size is 0.0166 deg. All of the velocity and the turbulence measurements inside the blade boundary layer were taken with a miniature cross-flow "V" hot-wire probe (TSI model 1240). The sensors were 3 μm diam platinum-tungsten wires with $\ell/d \approx 300$, located in the $(s-r)$ plane with their axis at 45 deg to the s axis. The s coordinate was parallel to the blade along a cylindrical surface and r was the radial coordinate. The probe was traversed normal to the blade surface. The details of the blade boundary measurements, as well as the experimental data and method of correcting the hot-wire data for any wall vicinity effects, are given in Ref. 6.

LDV Measurement Technique for the Inviscid Flow Data

A single-channel laser Doppler velocimeter (LDV) with on-axis backscatter light collection was used to measure the flowfield away from the blade surfaces. The system operated with 4 W argon-ion laser tuned for the green line. The entire system, comprised of the laser and transmitting and receiving optics, was mounted on an x-y-z traversing table. The three linear degrees of freedom, with the possibility of tilting the table, enabled positioning of the bisector of the beam accurately in the radial location.

Only one component of the velocity lying on the plane of the beam, but perpendicular to the bisectors of the beam, could be measured with a single-channel LDV. Hence, the measurement of either the tangential or the axial velocity component was made by rotating the plane of the beam. This was achieved by rotating the beam splitter.

The transmitting optics considered of a beamsplitter, a 3.75 X beam expander, and a 152 mm diam front lens with a focal length of 762 mm. The half-angle of the intersecting beam was measured to be 3.12 deg and provided a probe volume diameter of 0.111 mm and a probe volume length of 2.03 mm, based on the $1/e^2$ intensity points. The scattered light from the particles passing the probe volume was received by the front lens and directed to be photomultiplier through a field stop unit and a receiving assembly. The field stop consisted of a focusing lens, an aperture of 0.2 mm diam, and a filter. A beam splitter was used to orient the fringe pattern at ± 45 deg with response to the compressor axis.

A quartz window of 25.4 diam and 6.35 mm thick was used to transmit the laser beams to the rotor passage. The diameter of the quartz window was much smaller than the radius of curvature of the outer casing. Hence, no problems were encountered in matching the quartz window with the outer casing. The quartz window was also coated with an antireflective coating, which helped in reducing the glare from the wall. In addition, the rotor was coated with an orange fluorescent enamel (Deristo C-GLO 913 Red). During the experimental investigation, the rotor intercepted the laser beam and scattered an orange light. The scattered light collected by the receiving optics was comprised of real signal (green in color) scattered by the seed particle and the noise (orange in color) scattered by the rotor. An orange filter used just prior to the directing of the scattered light on the photomultiplier helped to filter out the orange background noise. The orange filter had a peak transmittance of 80% at a central wavelength of 514.5 nm and a half-bandwidth of 6.4 nm. This procedure helped to reduce the background noise drastically.

The flow was seeded with an atomized (0.6-2 μm) spray of mineral oil that was injected into the flow usptream of the rotor.

LDV Data Processing and Error Estimate

For processing the enormous amount of data generated (at high speed), a countertype signal processor was interfaced with an HP 2100S computer. The signal from the photomultiplier tube was fed into the counter, if necessary, through a frequency shifter. The signal was validated and digitized. Both the analog and digital signals were generated by the processor. The processor records were time referenced to a once-per-revolution pulse it received from the photodetector mounted on the rotor shaft. This photodetector looked at a timing reference mark on the rotor, a process that helped to tag the valid data with the angular position of the rotor. Each of the processed data points represented the Doppler frequency shift associated with the respective tangential location for a passage. The maximum number of circumferential measure-

Table 1 Rotor blade element details

Radius ratio	0.5	0.6	0.7	0.8	0.9	1.0
Chord, cm	12.39	12.68	13.25	13.68	14.41	15.41
Blade spacing, cm	6.97	8.37	9.60	11.15	12.55	13.94
Max thickness, % chord	9.5	9.1	7.6	6.5	5.9	5.1
Stagger angle, deg	22.5	26.0	28.5	34.0	39.0	45.0

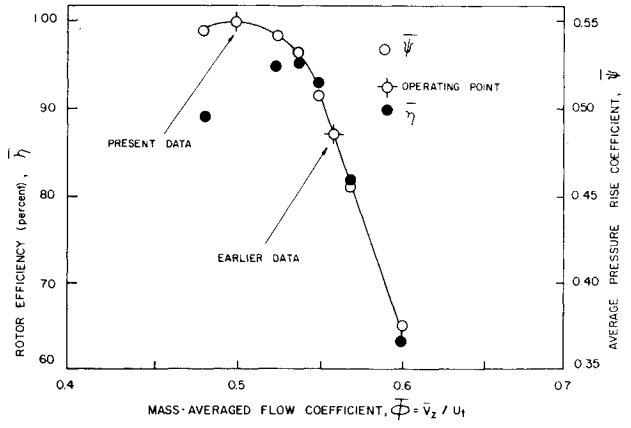

Fig. 1 Overall performance of the compressor rotor.

ment locations across the passage was 145. Even though the data are available at all these locations, only 17 measurement points are used in presenting the blade-to-blade variation of velocity here.

During the data acquisition, a terminal was used to generate a graphic display of the data, which was updated at the end of the acceptance of 1450 data points. These data were acquired in 10 rotor blade passages at a fixed point in the absolute reference frame. Thus, the data were continuously monitored and terminated if necessary. The total number of measurment acquired is about 43,500 (or about 30 sets of measurement each with 1450 points).

Since the measurement location is fixed in absolute frame (same tip clearance, same upstream flow, etc.), the flow measured by the LDV in all 10 passages should be identical, unless the passages, blade profiles, and geometry differ from blade to blade. The data indicated no such nonuniformity. The unsteadiness caused by the guide vane wake or other upstream effects do not affect the results as the blade-to-blade distribution of the instantaneous velocities (except the random component due to turbulence) are identical in these passages. Hence, there are an adequate number of samples to derive the time-averaged velocity components. In most locations, where the LDV measurements are reported, the turbulence intensities were found to be about 2-4%, which gives rise to an error of less than 0.2% on the mean velocity. In the end wall region ($R=0.96$) away from the blade boundary layer, where turbulence intensities are high, the accuracy of mean velocity is about 0.5-1.0%.

The data reduction and the error analysis were very similar to those given in Refs. 9 and 10, so only a brief description is given here. The software package used in this measurement is the same as the one used in Ref. 11.

The data were taken with two different beam orientations and the Doppler frequency shift was converted to respective velocities by multipling it by the fringe spacing.

The error in locating the probe volume was ± 0.025 mm and the error in the beamsplitter setting was ± 0.03 deg. Error in the measurement arises due to: fluctuations in the flowfield and random noise due to photomultiplier tube, statistical or velocity bias, and angle of fringe bias. Error due to flow fluctuation and random noise from the photomultiplier tube depends on the background radiation and is difficult to estimate.

Fluctuation in the flow may be caused by a drift in the rotor speed, which in this study was nearly 0.18%. Other causes of flow fluctuation are the turbulence and gradient in velocity, which was discussed earlier. Error due to velocity gradient was assumed to be negligible, since LDV was employed for measurements away from both the wall and the blade surfaces. The velocity or statistical bias is introduced by the variation of the data rate. A high data rate causes a higher measured value than the true measurement. An estimate of the error due to statistical bias was less than 1% based on analysis in Refs. 9 and 10.

The error termed as fringe or angle bias occurs when the flow is not parallel to the plane of the laser beams. The factor controling the fringe bias is the ratio N/N_{fr}, where N is the minimum number of cycles required by the signal processor and N_{fr} the number of measurable fringes. The fringe bias can be minimized by reducing the N/N_{fr} ratio. The use of frequency shift is an effective means of minimizing the fringe bias. In the present study, the fringe bias was maximum in the end-wall region, which was minimized by decreasing N.

Experimental Results and Interpretation

The measurements reported in this paper were carried out at six axial and five radial locations in the rotor blade passage. The locations for which the data are reported in this paper are listed in Table 2. The axial distance was normalized by the local blade chord length (C); $Z=0$ corresponds to the leading edge and $Z=1$ to the trailing edge. The radial distance from the compressor axis was normalized by the rotor tip radius. The rotor tip speed ($U_t=53$ m/s) was used to normalize the measured values of the velocities.

The radial variation of the inlet flow properties at $Z=0.72$ upstream of the rotor is shown in Fig. 2. The measurements were taken at midpitch of the IGV. Since the measurement location is far downstream of the IGV, where the wake defects are found to be extremely small, the results are very close to the average values. The inlet flow measurements were performed with a stationary wedge probe.

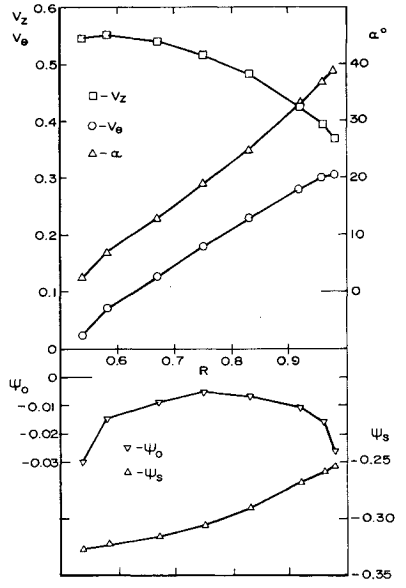

Fig. 2 Inlet flow propeties upstream of the rotor leading edge at off-design condition ($\phi=0.50$).

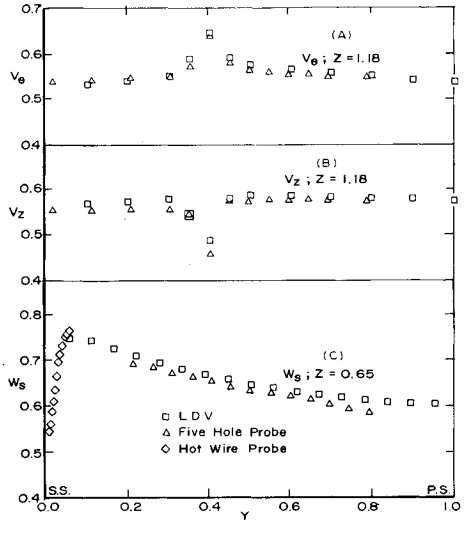

Fig. 3 Comparison of LDV, five-hole probe, and hot-wire probe data at $R=0.75$.

Table 2 Axial and radial measuring locations

R	Z						mm, C	mm, S
0.58	−0.02	0.23	0.45	0.62	0.81	1.02	126	81
0.75	−0.02	0.24	0.47	0.65	0.84	1.02	134	104
0.92	−0.02	0.26	0.52	0.73	0.93	1.02	146	128
0.96	−0.02	0.28	0.53	0.74	0.94	1.02	150	131

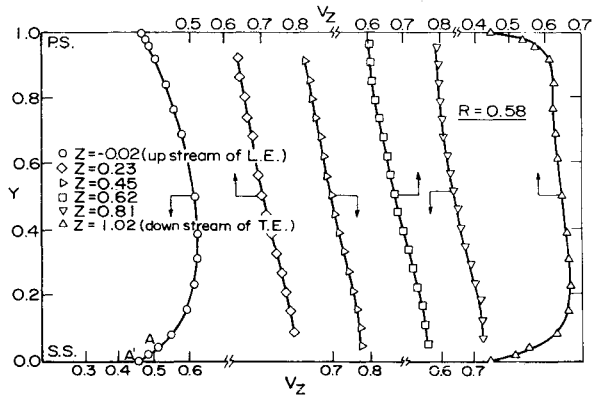

Fig. 4 Blade-to-blade variation of axial velocity, $R=0.58$.

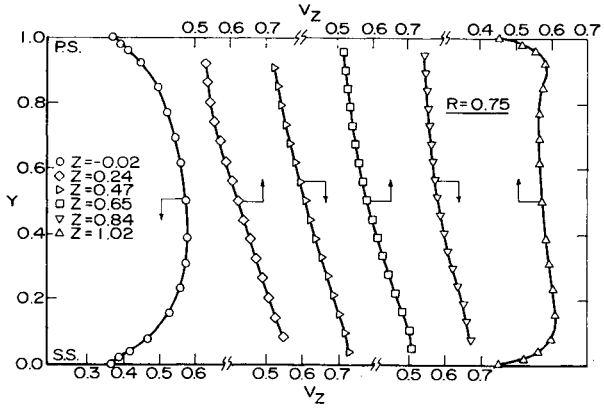

Fig. 5 Blade-to-blade variation of the axial velocity, $R=0.75$.

Comparison of LDV, Two-Sensor Hot-Wire, and Five-Hole Probe Data

To validate the LDV data, the measurements were also performed with conventional probes (five-hole and two-sensor hot-wire probes) at several locations inside and outside the passage. The details on the probe, instrumentation, and data acquisition system can be found in Ref. 5. The agreement between the measured axial and the tangential velocities, acquired from the LDV and the five-hole probe downstream of the trailing edge ($Z=1.18$), is excellent, as shown in Figs. 3a and 3b. The blade-to-blade distribution of the streamwise velocity inside the passage at location $R=0.75$, $Z=0.65$ is shown in Fig. 3c. The blade boundary measurement on the suction surface was derived from the hot-wire measurement. The agreement of the three sets of measurements was very good. The maximum difference was about 3% near the pressure side. The comparisons shown in Fig. 3 provide a validation of the present data acquired with an LDV system.

Axial Velocity Profiles

The blade-to-blade variation of the axial velocity profiles at various axial (or chordwise) locations is shown in Figs. 4-7 for $R=0.58$, 0.75, 0.92, and 0.96, respectively.

The data at $Z=-0.02$ (just upstream of the leading edge) show the major effects of the leading edge; all were inviscid in nature. The presence of a stagnation point on the leading edge, and its effect in decelerating the flow in the vicinity of the leading edge, is dramatically illustrated in these figures. Similar results have been reported in transonic compressor rotors.[10,12] The leading-edge effect is similar in its general characteristics both for low-speed rotors and for high-speed rotors having detached bow shocks. The deceleration of the flow near the leading edge and the acceleration away from it

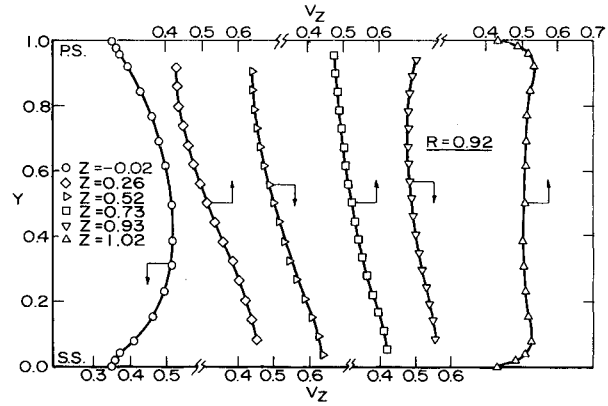

Fig. 6 Blade-to-blade variation of the axial velocity, $R=0.92$.

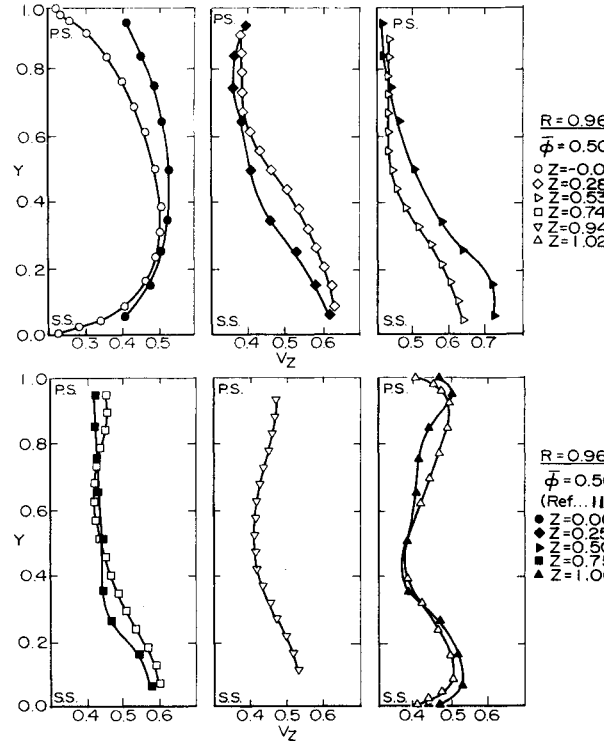

Fig. 7 Blade-to-blade variation of the axial velocity, $R=0.96$.

are evident at all radii. It is also evident that maximum velocity gradients (in inviscid flow) occurred near the leading edge. The gradients were much higher near the suction side; this high-velocity gradient region extended to about 20% of the blade spacing in the tangential direction from the leading edge. The radial location $R=0.96$ had the largest velocity gradient near the suction surface of the leading edge. This may have been caused by higher incidence (than the design) at this location due to the presence of the annulus wall boundary layer.

The axial velocity distribution inside the blade passage was almost linear in the blade-to-blade direction. It should be emphasized here that no data were available inside the blade boundary layer and the observed flowfield was primarily inviscid in nature, except the flow in the tip region ($R=0.96$). At $R=0.96$, the effects of viscosity and the mixing of the leakage flow resulted in a nonlinear distribution of the velocity in the blade-to-blade direction. The maximum streamwise velocity gradients ($\partial V_z/\partial s$) occurred from the leading edge of the blade to about midchord, especially near the suction surface. The streamwise gradient in velocity is

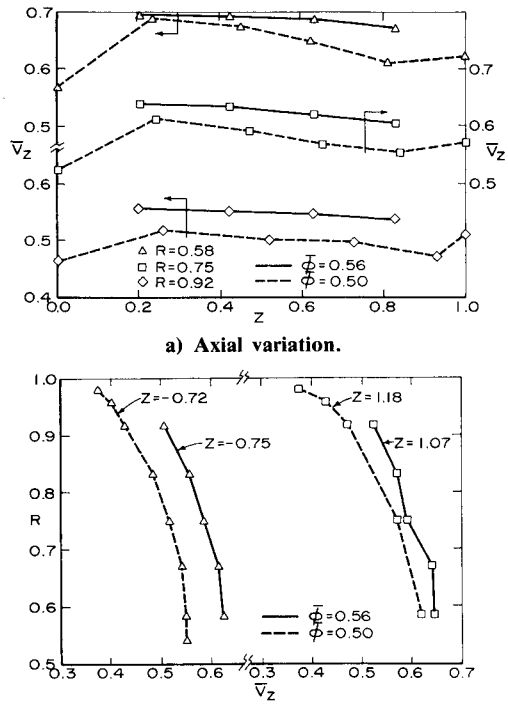

a) Axial variation.

b) Radial variation.

Fig. 8 Axial and radial variation of average axial velocity at design and off-design conditions.

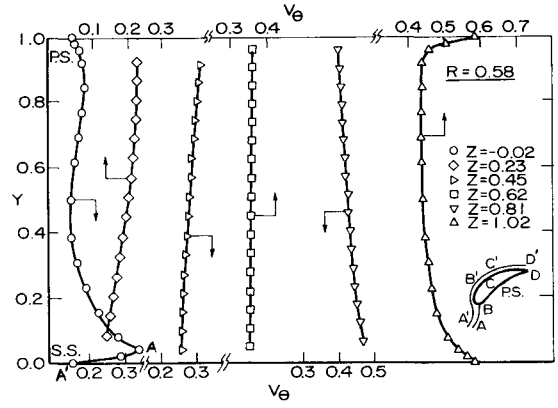

Fig. 9 Blade-to-blade variation of absolute tangential velocity, $R=0.58$.

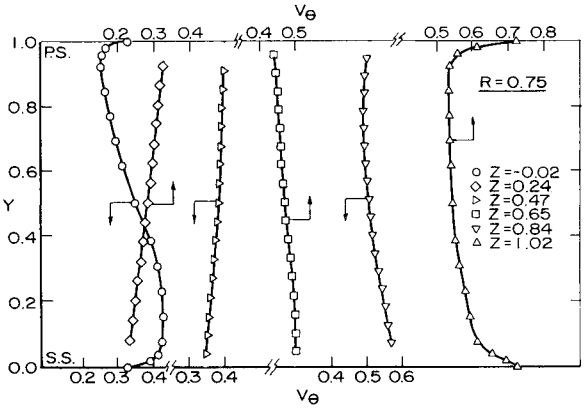

Fig. 10 Blade-to-blade variation of absolute tangential velocity, $R=0.75$.

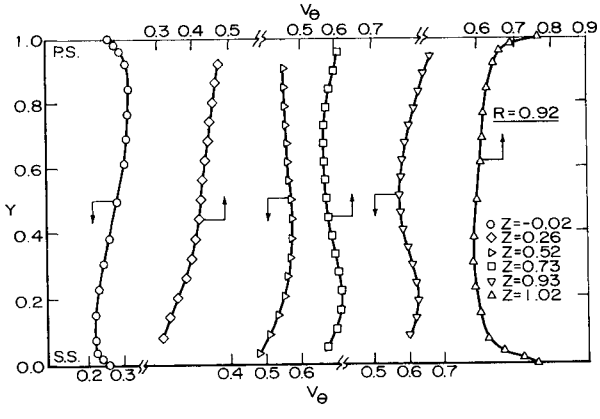

Fig. 11 Blade-to-blade variation of absolute tangential velocity, $R=0.92$.

mild near the pressure surface (except from $Z=-0.02$ to 0.25) and beyond $Z=0.5$.

The change in axial velocity near the suction surface from the leading edge to the quarter-chord location was very rapid, as much as 100% in most locations and neary 200% at $R=0.96$ (Fig. 7). A well-defined wake was observed at $Z=1.02$, a station very close to and downstream of the trailing edge. The wake was wider on the suction side.

All the phenomena observed in these measurements were as expected, except the data near the leading edge (at all radii) and near the blade tip. The leading-edge phenomenon has been interpreted earlier. The profiles at $R=0.96$ showed unusual behavior. At this location, the profiles inside the blade passage were nearly uniform from the midpassage to the pressure surface, but showed unusually large gradients from the suction surface to the midpassage location.

The effect of the tip clearance can be seen at $R=0.96$ (Fig. 7) beyond the midchord location. The tangential gradients in velocity were negligibly small from the midpassage to the pressure surface at most of the chordwise locations at $R=0.96$. This resulted from the leakage flow occurring in this region, which caused the tangential gradient of pressure to decrease. The defect in axial velocities near the midpassage, at $Z=0.53$ and beyond, was caused by the mixing of the leakage jet with the mainstream. Due to the blade motion, the leakage jet traveled farther away from the suction surface and the mixing between the leakage flow and mainstream occurred closer to the midpassage. This is contrary to the observations in a cascade, where the leakage jet tends to mix with the mainstream closer to the suction surface, causing a velocity (and kinetic energy) defect at that location.

The measurements from LDV[11] at $\bar{\phi}=0.56$ are shown compared with the present measurements ($\phi=0.50$) in Fig. 7. The axial locations of the measurements differ slightly. The measurements at the leading edge indicate that the effects were very similar at both flow coefficients; the discrepancy near the leading edge ($Z=-0.02$ at $\bar{\phi}=0.50$, $Z=0$ at $\phi=0.56$) was due to differing locations. The data in this region clearly reveal the presence of large velocity gradients that existed in the streamwise direction from $Z=-0.02$ to 0 along the blade surface. The velocity profiles are very similar at most other chordwise locations, even though the effect of the leakage flow was felt earlier along the chord in the case of $\bar{\phi}=0.50$. The flow near the trailing edge is similar in both cases.

Passage-Averaged Axial Velocities

The passage-averaged axial velocity ($\bar{\phi}=0.50$) is shown compared with the data at $\bar{\phi}=0.56$ in Fig. 8. It should be remarked here that the average values do not include the blade boundary layers. The axial velocities increased from $Z=-0.02$ to 0.2 (Fig. 8a) at all of the radial locations, an

increase consistent with those calculated from the blade blockage effect. The maximum values occurred close to the quarter-chord point, where the blade thickness was maximum. Beyond this chordwise location, there was a small decrease in the axial velocity. The velocity distribution was almost linear from $Z=0.2$ to 0.8, beyond which a small increase was observed. This is probably caused by the large boundary-layer growth that occurred between $Z=0.8$-1.0 on the suction surface. The $\bar{V}_z$ distribution at $\bar{\phi}=0.50$ was very similar to that observed at $\phi=0.56$. The data at $\bar{\phi}=0.56$ were taken from a five-hole probe[5] and hence no measurement was made at the leading edge. It is felt that the five-hole probe measurements were not accurate at this location due to flow interference and additional blockage effects caused by the probe.

The radial distribution of $\bar{V}_z$ at the inlet and at the exit of the rotor are shown in Fig. 8b. The inlet profiles are similar, differening only in magnitude. The exit profiles are also similar, but the data at $\bar{\phi}=0.50$ show a tendency toward a larger radial gradient in axial velocity as the blade tip was approached.

Absolute Tangential Velocity Profiles

The circumferential variation of the absolute tangential velocity V_θ is shown in Figs. 9-12 for $R=0.58$, 0.75, 0.92, and 0.96, respectively. As in the case of the axial velocity component, large circumferential gradients in V_θ occurred near the blade leading edge at all the radial locations.

The type of distribution observed near the leading edge ($Z=-0.02$) at $R=0.58$, shown in Fig. 9, is unusual and can be explained by comparing the flow variation along the stagnation streamline ABCD and a streamline close to the blade surface A′B′C′D′, as shown in the sketch in Fig. 9. The axial and relative tangential velocities decrease along the relative stagnation streamline AB, which results in a decrease in the axial velocity and an increase in the absolute tangential velocity at point A for $Z=-0.02$ as shown in Figs. 4 and 9. As the next streamline, such as A′B′C′D′, is approached ($Y\cong 0$), the relative tangential velocity increases and hence the absolute tangential velocity decreases along the tangential direction. Furthermore, the relative flow angle increases for streamline A′B′ when compared with the streamline AB, providing a further increase in the relative tangential velocity (or decrease in the absolute tangential velocity). This accounts for a decrease in V_θ at A′ for $Z=-0.02$ (Fig. 9). Furthermore, an increase in the relative flow angle has a dominant effect on the axial velocity, decreasing its value as shown at A′ in Fig. 4. This is probably the most plausible explanation of the observed behavior.

The circumferential gradient in V_θ was large from the leading edge to $Z=0.23$ at $R=0.58$, decreasing gradually to zero at $Z=0.62$. Beyond $Z=0.62$, there was a reversal of the velocity gradient, brought about by the deceleration of the relative flow or acceleration of the absolute flow near the suction surface. As the trailing edge was approached, V_θ became uniform again in the circumferential direction.

The data at $R=0.75$ (Fig. 10) is very similar to those at $R=0.58$. The distribution of V_θ at $Z=-0.02$ is rather unconventional. The effects observed at this axial and radial location are not as strong as those measured at the corresponding location for $R=0.58$. One possible reason for this is that the flow near the hub sees a much higher incidence due to the presence of the hub wall boundary layer and the stagnation point there is located closer to the pressure surface, while the incidence at $R=0.75$ is close to the design and hence the effects are not as dominant. But the observed behavior, namely, an increase in V_θ away from the blade surface, is due to reasons given earlier for the V_θ distribution at $R=0.58$, $Z=-0.02$.

The tangential velocity distribution at $R=0.92$ (Fig. 11) shows the usual inviscid trend from $Z=-0.02$ to 0.26. The distribution at $Z=0.52$ shows uniformity in V_θ distribution, except near the suction surface. At and beyond $Z=0.73$, the effect of leakage flow is seen. The overturning observed near the suction surface at $Z\geq 0.73$ may be due to roll back of the leakage jet toward the suction side.

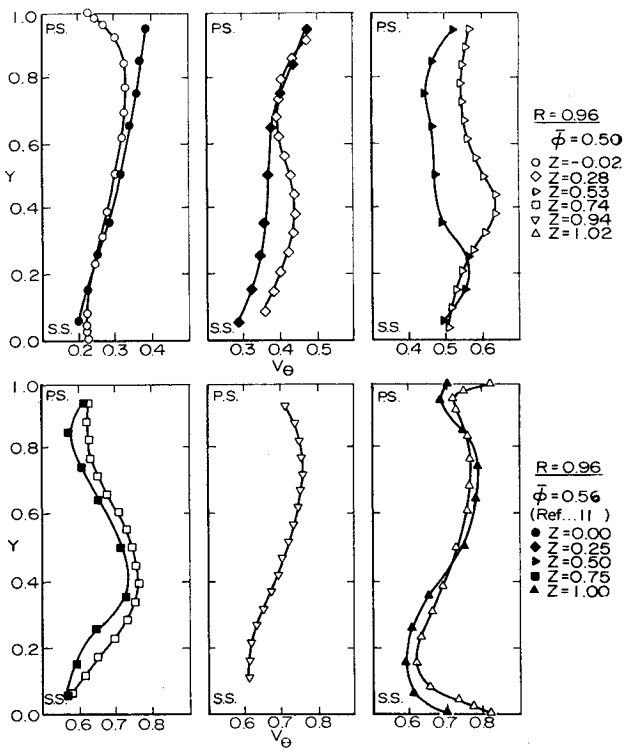

Fig. 12 Blade-to-blade variation of absolute tangential velocity, $R=0.96$.

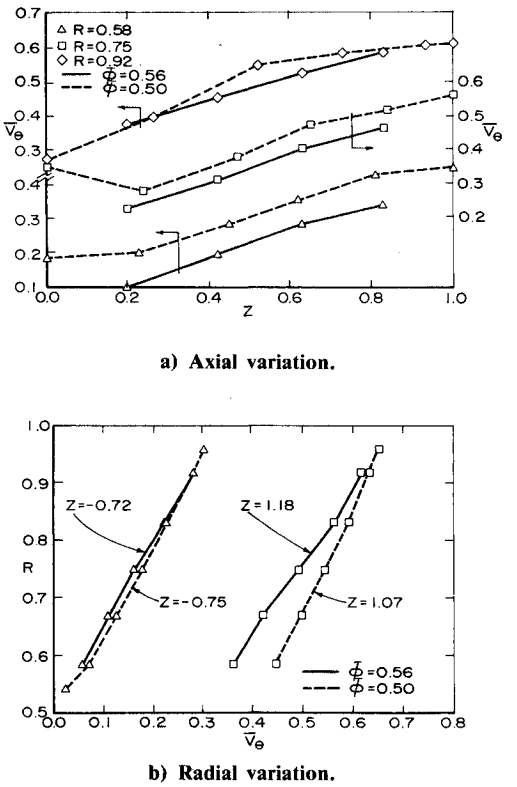

a) Axial variation.

b) Radial variation.

Fig. 13 Axial and the radial variation of average tangential velocity at design and off-design conditions.

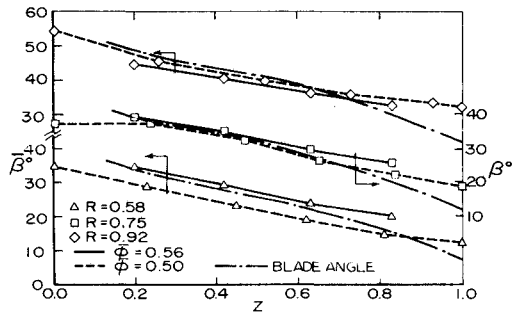

a) Axial variation.

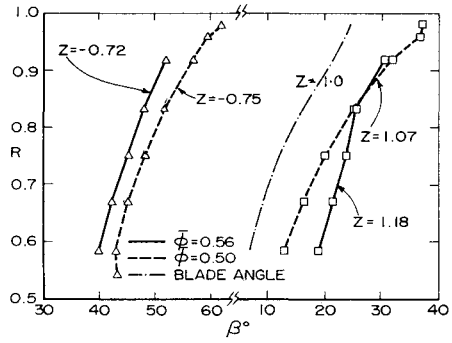

b) Radial variation.

Fig. 14 Axial and radial variation of average flow angle at design and off-design conditions.

The tangential velocity distribution at $R=0.96$ (Fig. 12) shows the complex nature of the flow in this region and is consistent with the axial velocity distribution shown in Fig. 7. The distribution at $Z=-0.02$ was as expected in an inviscid flow. The V_θ distribution deteriorated gradually as the flow progressed downstream. The comparison with V_θ distribution at the two operating conditions ($\bar{\phi}=0.50$ and 0.56) shows that the influence of the leakage flow near the quarter-chord point ($Z=0.23$-0.28) was negligible for $\bar{\phi}=0.56$ and substantial for $\bar{\phi}=0.50$. This was expected, due to higher blade loading and higher suction pressures for the $\bar{\phi}=0.50$ case. The effect of the leakage flow was to underturn the flow near the pressure and the suction surfaces, resulting in a decreased value of V_θ in these regions. This is evident from V_θ distribution shown in Fig. 12 for $\bar{\phi}=0.50$ and 0.56. The V_θ distribution at $Z=0.53$ seems to indicate that the leakage flow was much more dominant for $\bar{\phi}=0.50$. The distribution of V_θ was similar for both flow coefficients at $Z=0.74$-1.02. It is evident that the flowfield was dominated by the leakage flow effects at this radius and that the leakage flow effects were much stronger for $\bar{\phi}=0.50$, especially from the leading edge to the midchord.

Passage-Averaged Tangential Velocities (V_θ)

The axial variation of the blade-to-blade mass-averaged tangential velocity $\bar{V}_\theta$ at $\bar{\phi}=0.50$ and 0.56 is shown in Fig. 13a. It should be remarked here that the averages do not include the blade boundary layer. The data for $\bar{\phi}=0.56$ were taken with a five-hole probe for various radii. The distribution of V_θ near the hub shows almost a linear variation for $Z=0.2$-0.8, with a much smaller change in V_θ near the leading- and trailing-edge regions. At $R=0.75$, as mentioned earlier, some unusual behavior was observed far upstream. The values of $\bar{V}_\theta$ increased from 0.2 at $Z=-0.72$ to 0.35 at $Z=-0.02$, decreasing to 0.3 at $Z=0.02$ for $\bar{\phi}=0.50$. Beyond $Z=0.2$, $\bar{V}_\theta$ increased almost linearly until $Z=1.0$. The distribution at $Z=0.92$ shows a linear increase up to $Z=0.53$, beyond which very little change in V_θ can be observed. The distributions for $\phi=0.50$ and 0.56 were very similar, even though the magnitudes were generally lower for the latter case.

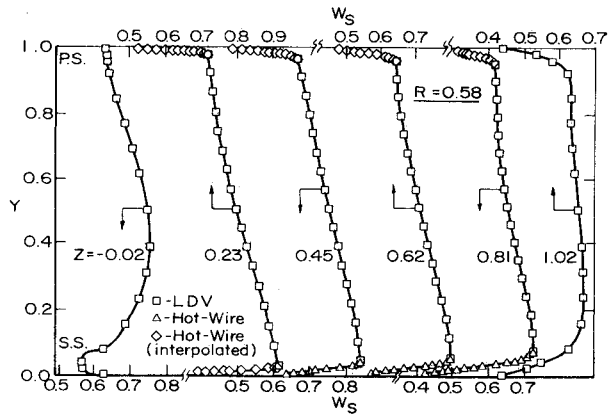

Fig. 15 Composite velocity profiles (W_s) at $R=0.58$.

The radial variation of $\bar{V}_\theta$ (Fig. 13b) shows almost identical distribution at the inlet, but substantially different distribution at the exit at the two flow coefficients tested. The flow turning was much higher at $\bar{\phi}=0.50$ in the hub wall and the midspan regions and nearly the same in the tip region ($R=0.9$-1.0).

Flow Angles

The passage-averaged flow angles are shown in Fig. 14. The flow turning from inlet to exit was almost linear at all the radial locations. The radial distribution at the exit shows that the deviation angles were lower for $\bar{\phi}=0.50$ for most radial locations, but the same in the tip region (beyond $R=0.85$). The blade angles shown in Fig. 14 are the local angles of the camber line.

Streamwise Velocity Profiles

The resultant of the axial and relative tangential velocity, denoted by W_s, ($=\sqrt{W_\theta^2+W_z^2}$), is derived from the LDV data acquired away from the surfaces and the hot-wire data acquired near the blade surfaces. In many instances, the axial location where the hot-wire data were acquired was different from the axial measuring station at which the LDV data were measured. In such a case, the data from the hot-wire probe were interpolated from the measurement at various axial locations. The results are shown plotted in Figs. 15-17 for $R=0.58$, 0.75, and 0.96, respectively. These figures represent a composite of velocity plots from the leading to the trailing edges and from the suction to the pressure surfaces, including the blade boundary layers.

It is clear from Figs. 15-17 that the blade blockage and the leading-edge effects, as discussed earlier, were also present in this case.

At $R=0.58$ (Fig. 15), the inviscid region was well behaved, with the usual linear variations of W_s in the circumferential direction. The boundary-layer growth was small at $Z=0.23$ on both surfaces. The boundary-layer growth was larger on the suction surface, with the major growth occurring beyond the midchord location. The behavior at $R=0.75$ was very similar to that observed at $R=0.58$. Major changes were observed in the distribution of W_s at $R=0.96$. The boundary-layer growth was large on both the surfaces, which was caused by the transport of the blade boundary layer toward the blade tip. Furthermore, the effect of the tip clearance (or the leakage flow) can be clearly seen in the loss of kinetic energy of the mean flow ($W_s^2/2$) near the midpassage. As indicated earlier, intense mixing between the main flow and the leakage flow (which travels farther away from the suction surface than a stationary cascade) resulted in velocity deficiencies at this location. The results[5] at $\bar{\phi}=0.56$ show a very similar trend, both qualitatively and quantitatively.

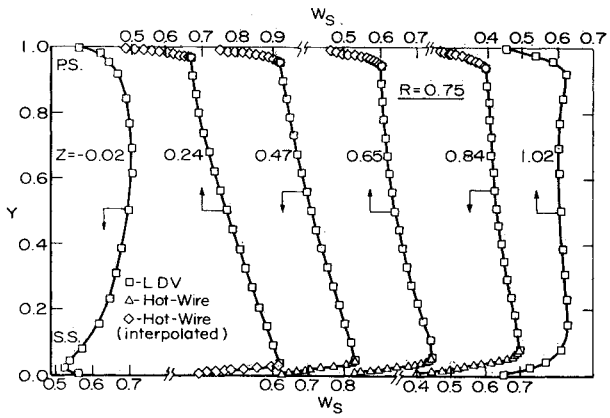

Fig. 16 Composite velocity profiles (W_s) at $R=0.75$.

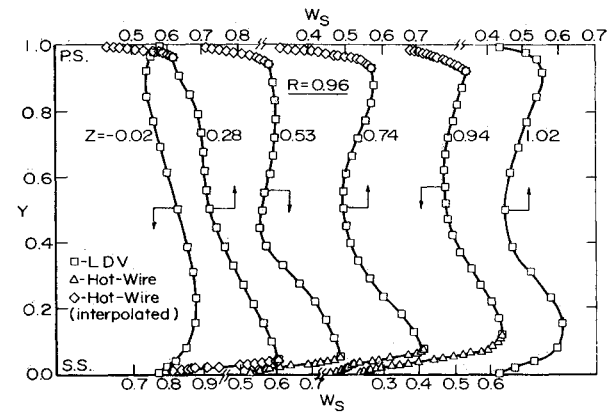

Fig. 17 Composite velocity profiles (W_s) at $R=0.96$.

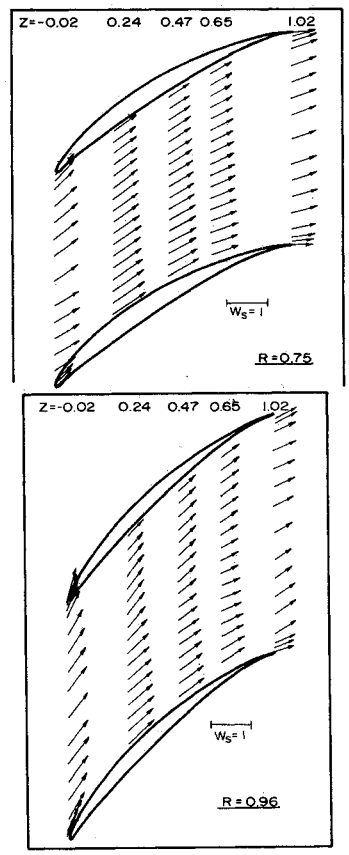

Fig. 18 Total velocity vectors at $R=0.75$ and 0.96.

The velocity vectors (W_s) lying in the cascade plane at $R=0.75$ and 0.96 are shown in Fig. 18. At $R=0.75$, the effect of the leading edge in decelerating the flow and the substantial redistribution occurring near the trailing edge can be seen clearly. The velocity vectors at other locations were well behaved. The leading- and trailing edge effects mentioned above were also evident at $R=0.96$. Furthermore, the effect of the leakage flow in changing the magnitude and the direction of the velocities, inside the passage and away from the blade surfaces, is also clearly evident from these vector plots.

Conclusions

Some of the important conclusions derived from the present investigation reported in this paper are as follows:

1) In the inviscid regions of the rotor passage, the nature of the flow is similar at both the design and off-design conditions.

2) One of the significant results from this study is the observed effect of the leading edge on both of the velocity components. Large velocity gradients are observed in the streamwise and tangential directions in the vicinity of the leading edge.

3) The velocity profiles, from blade to blade, are almost linear (except near the leading edge) up to about 8% of the span from the blade tip.

4) A very complex flow, resulting from the interaction of the leakage flow with the main flow, has been observed at $R=0.96$. The leakage flow seems to travel farther into the passage, resulting in substantial deficiencies in the axial and total (relative) velocity components. The absolute tangential velocity distribution at this location seems to indicate large underturning near the pressure and suction surfaces.

5) The deviation angle is nearly constant at all the radii at the off-design condition, but increases toward the hub region at the design condition.

Acknowledgment

The first author was a Fulbright Scholar during 1983-84 and was supported by the U.S. Council for the International Exchange of Scholars (CIES) through Grant 83-03827. The authors also wish to thank K.N.S. Murthy and J. Fetterolf for their help with the instrumentation setup.

References

[1]Katsanis, T. and McNally, W. D., "Revised Fortran Program for Calculating Velocities and Streamlines on the Hub and Shroud Mid-Channel Stream Surface of an Axial- Radial-, or Mixed-Flow Turbomachine or Annular Duct," NASA TND 8430/1, 1977.

[2]Katsanis, T., "Fortran Program for Calculating Transonic Velocities on a Blade-to-Blade Surface of a Turbomachine," NASA TND 5427, 1969.

[3]Denton, J. D., "A Time Marching Method for Two- and Three-Dimensional Blade to Blade Flows," British Aircraft Research Council R&M 3775, 1975.

[4]Pierzga, M. J. and Wood, J. R., "Investigation of Three-Dimensional Flow Field Within Transonic Fan Rotor: Experiment and Analysis," *Journal of Engineering for Gas Turbines and Power*, Vol. 107, No. 2, April 1985, p. 436.

[5]Pouagare, M. and Lakshminarayana, B., "Three-Dimensional Flow Field Data in a Low Speed Axial Flow Rotor Passage," submitted for publication as NASA CR, 1986.

[6]Pouagare, M., Galmes, J. M., and Lakshminarayana, B., "An Experimental Study of the Compressor Rotor Blade Boundary Layer," *Transactions of ASME, Journal of Engineering for Gas Turbines and Power*, Vol. 107, April 1985, pp. 364-373.

[7]Lakshminarayana, B., "An Axial Flow Research Compressor Facility Designed for Flow Measurement in Rotor Passages," *Journal of Fluids Engineering*, Vol. 102, Dec. 1980, pp. 402-411.

[8]Smith, L. H., "Three Dimensional Flow in Axial Flow Turbomachinery," WADC Rept. 55-348, Vols. I, II, March 1956.

[9]Powell, J. A., Strazisar, A. J., and Seasholtz, R.G., "Efficient Anemometer for Intra-Rotor Flow Mapping in Turbomachinery," *Transactions of ASME, Journal of Engineering for Power*, Vol. 103, 1981, pp. 424-429.

[10]Strazisar, A. J. and Powell, J. A., "Laser Anemometer Measurements in a Transonic Axial Flow Compressor Rotor," *Transactions of ASME, Journal of Engineering for Power*, Vol. 103, 1981, pp. 430-437.

[11]Murthy, K.N.S. and Lakshminarayana, B., "Laser Doppler Velocimeter Measurement in the Tip Region of a Compressor Rotor," *AIAA Journal*, Vol. 24, May 1986, pp. 807-814.

[12]Schodl, R., "A Laser Two Focus Velocimeter for Automatic Flow Vector Measurements in the Rotating Components of Turbomachines," *Journal of Fluids Engineering*, Vol. 102, Dec. 1980, pp. 412-419.